Remote Sensing of the Global Environment with Satellite Scatterometry

Son V. Nghiem* and Gregory Neumann

Jet Propulsion Laboratory, California Institute of Technology, MS 300-235, 4800 Oak Grove Drive, Pasadena, CA, USA 91109

ABSTRACT

This paper presents an overview of satellite scatterometry for remote sensing of the global environment from the tropics to polar regions. Results were derived from microwave backscatter data acquired by the NASA SeaWinds scatterometer aboard the QuikSCAT (QSCAT) satellite. QSCAT observed two successive super cyclones that hit the Orissa coastal region of India, affecting 15 million people in 1999. The extent of soil moisture change was delineated after Cyclone Nargis made landfall in Myanmar in May 2008. QSCAT detected excessive rainwater followed by a severe drought leading to widespread wildfires in California, U.S., in 2007. QSCAT tracked vegetation change in an extreme drought in Nairobi, Kenya, affecting 3 million people in 2000. QSCAT monitored snowmelt patterns over the Northern Hemisphere, which showed poleward oscillations of melt bands. QSCAT revealed a record reduction in Arctic perennial sea ice in this decade and a further drastic decline of perennial ice in 2008. At 1-km posting, QSCAT identified urban and suburban areas where backscatter was shown to correlate with population density. QSCAT delineated wind shadow areas near small islands in the Asia-Pacific region and persistent wind patterns for offshore wind power development. These results demonstrate that satellite scatterometer can provide numerous crucial data products to the Global Earth Observation System of Systems.

Keywords: Scatterometer, cyclone, soil moisture, vegetation, flood, drought, snowmelt, sea ice, urban, wind

1. INTRODUCTION

The QuikSCAT satellite was launched in June 1999. It carries the NASA SeaWinds scatterometer, which is an accurate and stable radar operated at the Ku-band frequency of 13.4 GHz. QSCAT accurately measures global backscatter (~0.2 dB accuracy, 3σ) with an 1800-km swath for the vertical (V) polarization and a 1400-km swath for the horizontal (H) polarization[1]. QSCAT measurements cover more than 90% of the Earth's surface. With the frequent and large-scale coverage, QSCAT data are useful for remote sensing of the global environment and for monitoring environmental change in this decade. We have developed innovative methods using QSCAT data for observations of cyclone impact, soil moisture, vegetation, drought, snowmelt, sea ice, urban and suburban areas, wind shadow, and persistent wind patterns in offshore waters. These results are presented in this overview paper.

2. CYCLONES AND FLOODS

QSCAT provides near-daily global coverage with the capability to see through clouds and darkness. Developing a technique for the delineation of water inundation using global scatterometer data is appropriate and highly relevant to the timely coverage requirement for flood applications. We use an innovative technique based on the polarization reversal of radar backscatter to detect inundated areas[2], which compared well will results from Moderate Resolution Imaging Spectroradiometer data. The method is based on relative backscatter between V and H polarizations, and does not require the use of absolute backscatter. An important advantage is that an inundated area can be detected when dual polarized data are collected without waiting for multi-temporal revisits as required by the change-detection method.

In 1999, strong cyclones and severe widespread floods occurred over several countries in the Asian summer monsoon region. Heavy monsoon rains starting in June devastated large areas of Asia in the summer of 1999. With our flood mapping approach, QSCAT data acquired over Asia showed extensive floods in Anhui, Zhejiang, Jiangsu, and other

*Son.V.Nghiem@jpl.nasa.gov; phone 1 818 354-2982; fax 1 818 393-3077

provinces in the Yangtze River basin[2].   According to reports from the United Nations Office for the Coordination of Humanitarian Affairs (UN-OCHA), 100 million people in China were affected by floods in 1999.   QSCAT data over India detected the North Bihar flood. Triggered by torrential monsoon rains, this flood was the worst in more than a decade; it affected 5 million people and inundated more than 2700 villages in 21 districts.

From July 1999, the scatterometer flood mapping indicated that the flood situation in India had worsened and spanned extensive regions from West Bengal, through Bihar, to Uttar Pradesh, and up to Himachal Pradesh. In October 1999, time-series of QSCAT wind and flood observations showed a cyclone forming over the ocean, moving toward land, making landfall, and causing extensive floods in the state of Orissa in eastern India. Another super cyclone hit Orissa again later, also in October, as seen in the satellite data, causing more intensive destruction in the coastal regions. The flood was worst in 100 years, affecting 15 million people[3]. The Orissa disaster was featured in the Public Broadcasting Service (PBS) special report *Cycle of Destruction* (a transcript from NewsHour with Jim Lehrer on 22 March 2000 can be found at http://www.pbs.org/newshour/bb/international/jan-june00/india_3-22.html).

To demonstrate the use of satellite scatterometry for flood monitoring, we present the case of the Orissa disaster[2]. Fig. 1 shows results for wind fields over the ocean and floods over Asia corresponding to the cases of the super cyclones discussed above. Different shades of blue correspond to the flood affected areas with different magnitudes of wetness and flood coverage. The topography overlaid on the maps reveals that the flood affected areas are determined by the local topographic characteristics. High-resolution topographic data can then be used to assess detailed flood susceptibility at small scales within the potential flood areas mapped by satellite scatterometer.
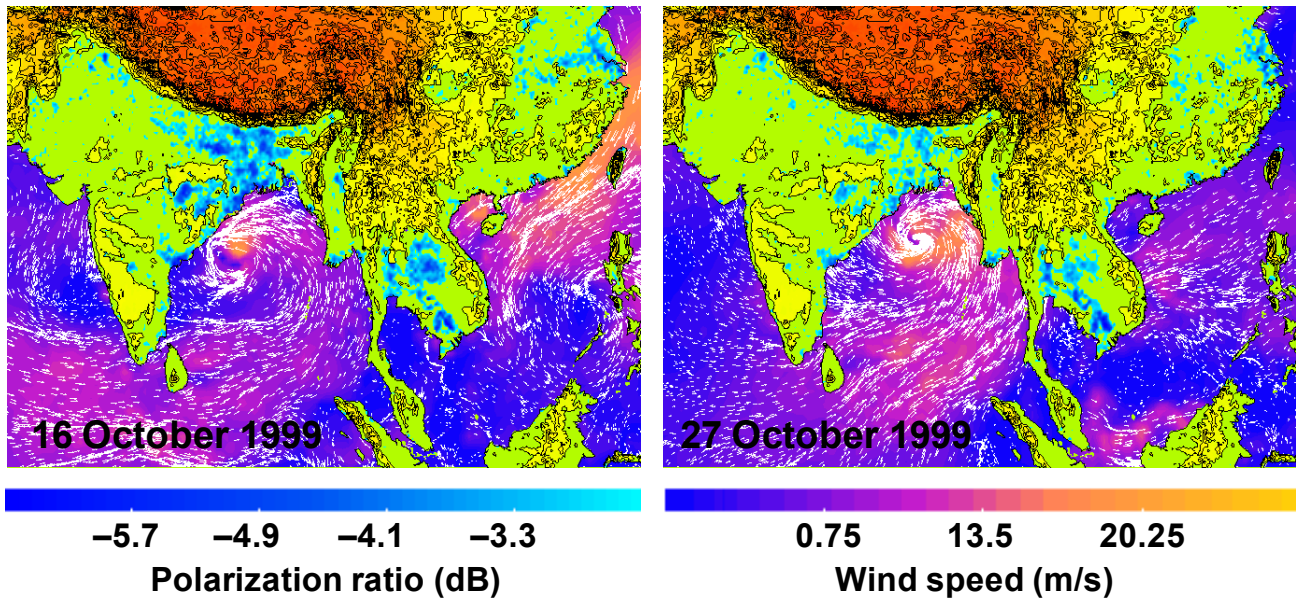

Fig. 1. The Orissa disasters: The left panel shows the first super cyclone and the right panel shows the second one. Different shades of blue over land represent different polarization-ratio values corresponding to different wetness or flood stages. Land topography is also plotted with colors from green to red for 500-5000 m, with a contour for every 500 m using the ETOPO5 dataset (http://www.ngdc.noaa.gov/mgg/global/etopo5.HTML). Over the ocean, the colors are for wind speed and the white arrows for wind direction.

Wind fields plotted over the ocean, also derived from QuikSCAT data, showed the wind speed and direction of the cyclones. In the image of the first cyclone (left panel of Fig. 1), more extensive wet areas were observed compared to the second one in the right panel of Fig. 1. Data of storm tracks showed that the first super cyclone (04B, October 1999) made landfall and invaded deep inland, causing extensive flooding over large areas. The second one (05B, October 1999) hit the Orissa coast and then moved back out to the ocean causing intensive coastal damages without extensive inland flooding.

Floods were also observed by QSCAT over many Asian countries in 1999 including Bangladesh, Nepal, Pakistan, Vietnam, Laos, Thailand, and Cambodia, with the worst flooding in 20 years[2]. It is important to map the extent of a

flood after it has already occurred because such information is crucial for flood relief efforts. Timely flood mapping provides data on the time, location, area, and number of affected people to support decision makers from local authorities such as fire and police departments, to national agencies such as the U.S. Agency for International Development (USAID) and the Federal Emergency Management Agency (FEMA), and international organizations such as the United Nations (UN) and the International Federation of Red Cross (IFRC). Such information will greatly help to efficiently allocate limited resources (food, medicine, and personnel) to flooded areas. Furthermore, flood mapping is important for scientific studies of regional flood hydrology, for assessing flood magnitude in comparison to preceding and subsequent events, and for agricultural and urban planning and development.

3. SOIL MOISTURE AND VEGETATION

The global water cycle is considered the most important of all biogeochemical cycles, where the surface evaporation, as a significant component of the water cycle, is also linked with heat and carbon cycles[4]. Acceleration of the global water cycle may lead to increased global precipitation, faster evaporation and a consequent exacerbation of hydrologic extreme. As a component of the global water cycle, measurements of soil moisture and its variability provide crucial data for hydrology research as well as operational applications to flood and drought monitoring and forecasting.

Traditionally, precipitation water is measured by rain gauge and surface radar (e.g., NEXRAD). Precipitation data are obtained by rain gauge observations from the Climate Prediction Center (CPC) and National Climatic Data Center (NCDC). It takes three to four months to assemble final, quality-controlled data. In the west, some climate divisions may have no stations reporting in a particular month or may lack a first- or second-order stations altogether. The use of rain gauge data from stations (point measurements) is a hit-or-miss approach and may not be representative of regional rainfall amounts. In this regard, timely measurements of the water distribution from precipitation over large spatial extent (areal data rather than point data) will be crucial to flood and drought monitoring.

Rain rate can also be estimated by surface radar such as NEXRAD. NEXRAD measures reflection from rain drops in the atmosphere (in a radar unit of dBZ). The surface radar data can be complicated to interpret with sufficient accuracy and coverage for wildfire applications due to altitude variations, terrain blockage (a very severe problem in mountainous California), multipath effects, and uncertainty in ice-liquid ratio. Absolute and cross calibrations among numerous individual radars located at different locations are not possible; consequently, local to regional biases are unknown. In California, there are about ten currently operational stations with seven stations deployed near the coast, leaving only three stations for the rest of the land (http://www.roc.noaa.gov/maps.asp). Furthermore, NEXRAD measurement of rain in the atmosphere is not representative of the precipitation amount that reaches the surface.

A different method to quantify precipitation amount is soil moisture change (SMC). This is a physical quantity that characterizes the precipitation amount that actually makes it to the surface and accumulates on land as an integrated parameter, as opposed to rain drops aloft in the atmosphere at any given time and space. We have developed and produced results derived from QSCAT to map patterns of land surface water accumulation from precipitation[5]. QSCAT surface water products are currently produced at JPL, and results compare well with precipitation data from NCDC Global Summary Of the Day (NCDC/GSOD) stations in the U.S., with soil moisture from the Soil Climate Analysis Network (SCAN) data in Arkansas, and with the NASA Land Data Assimilation System (LDAS) over the domain of the NASA Soil Moisture EXperiment (SMEX), including Iowa and the surrounding states[6].

Analyses of QSCAT data together with SCAN soil moisture data show two distinct temporal scales in the backscatter signature: the long-term scale variation corresponds to seasonal vegetation change[7], and the short-term transient response is related to SMC, induced by precipitation water on land surface. The seasonal signature in QSCAT backscatter data is highly correlated with the Normalized Difference Vegetation Index (NDVI), a characterization of greenness, derived from the satellite data collected by the Advanced Very High Resolution Radiometer (AVHRR) over the same area and the same time period. AVHRR NDVI has a correlation coefficient of 0.937 for the V polarization and 0.871 for the H polarization. As such, the QSCAT long-scale backscatter can measure NDVI. In fact, Ku-band backscatter was already shown to be related to NDVI[8], green leaf area index[9], and above-ground biomass[7], which are useful for estimating vegetation conditions. Results of QSCAT NDVI measurement at Nairobi in Kenya showed the collapse of a rain season in 2000 leading to a record low value of NDVI of 0.2, corresponding to an extreme drought that affected 3 million people. Another severe drought occurred again in Nairobi in 2005 as detected by QSCAT NDVI.
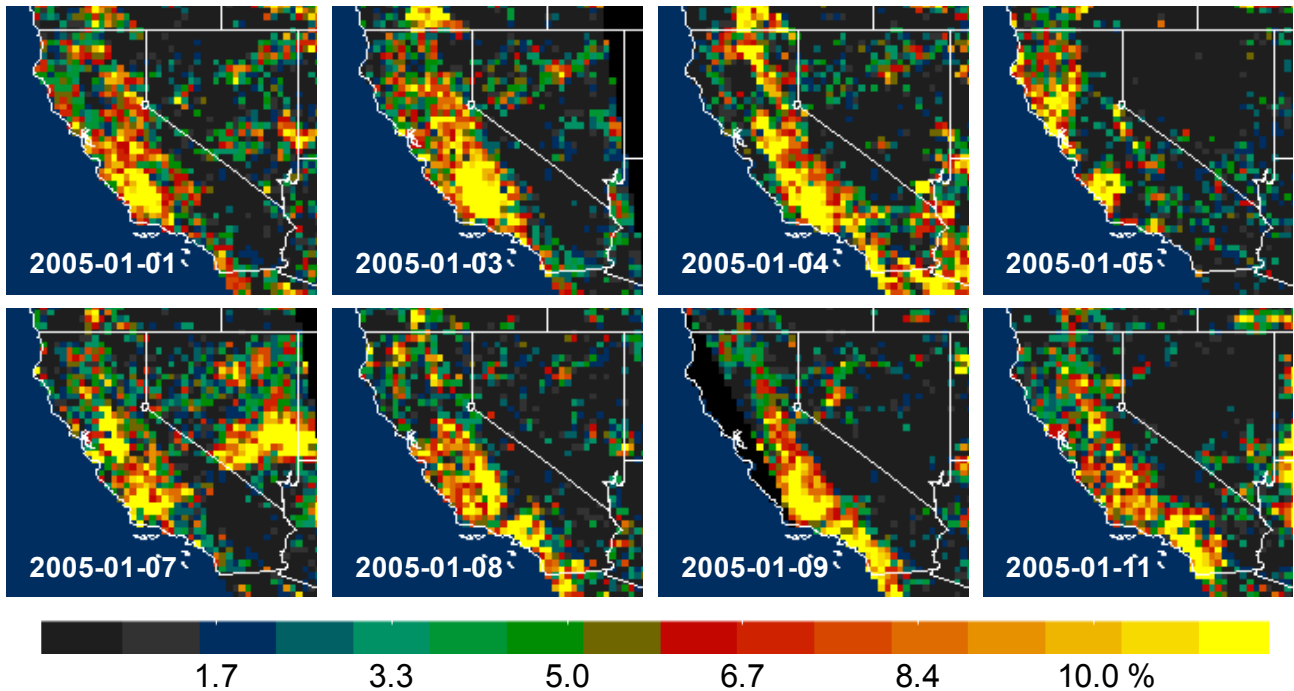
Fig. 2. Patterns of surface soil moisture change (SMC in terms of volumetric soil moisture percentage) over California in winter 2005 from precipitation brought by the moisture-laden storms from the 'Pineapple Express.' The color scale is volumetric SMC on each given date compared to the semi-monthly average. Yellow indicates more than 10% SMC and can be used to identify areas with excessive surface water potentially leading to soil saturation and flooding.
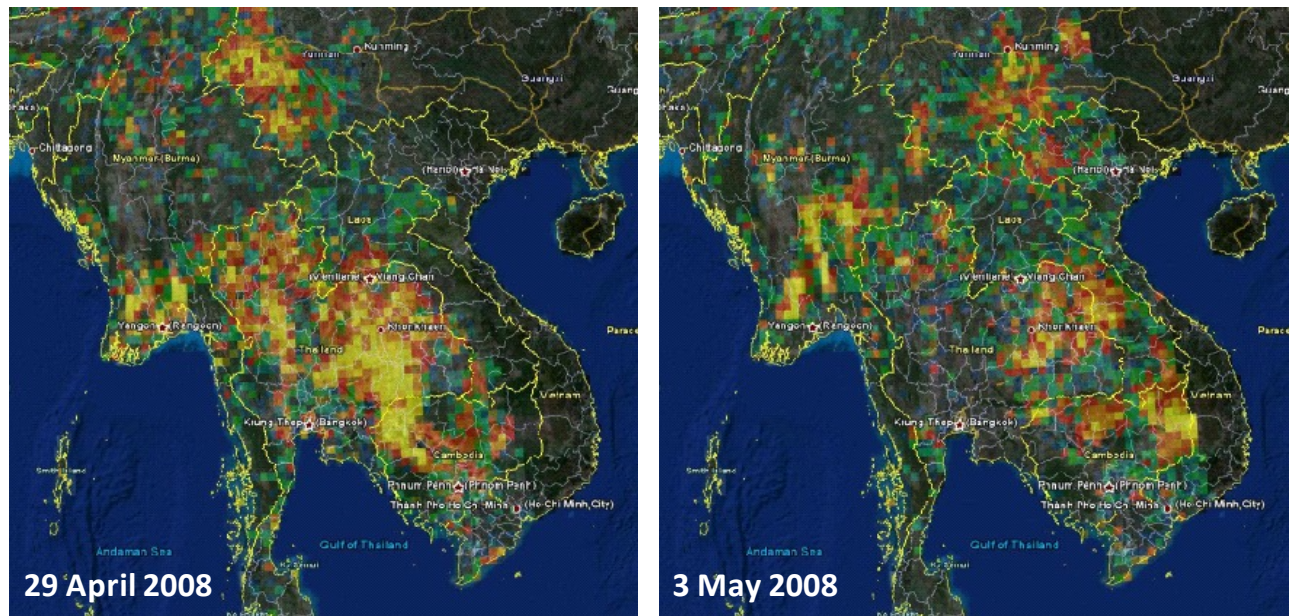

Fig. 3. SMC patterns measured by QSCAT on 29 April 2008 (left panel) and 3 May 2008 (right panel) before and after the landfall of Cyclone Nargis, respectively. SMC maps are overlaid on the NASA Blue Marble map together with country boundaries using Google Earth.

Relevant to precipitation amount is the short-term backscatter response to SMC associated with rainfall events. These are observed in the QSCAT transient backscatter signature characterized by an impulse increase due to the rainwater

input, followed by a gradual decrease in backscatter corresponding to the decrease in soil moisture. The gradual reduction is due to evaporation, soil infiltration, or other water-loss processes that may last a few days to a week or longer. QSCAT transient signatures still show a clear sensitivity to surface soil moisture at peak vegetation conditions during the summer months. Thus, the impulse response is useful to detect wetness events and to determine precipitation frequency at both low vegetation conditions (harvested or burned areas) and high vegetation states (heavy biomass loading). Analyses of QSCAT data and soil moisture measurements show correlation coefficients of 0.907 and 0.916, and standard deviations of 3.7% and 5.2% for vertical and horizontal polarization, respectively.

To illustrate the QSCAT capability to measure SMC, we present the case of extreme precipitation in California in the winter of 2005. A large-scale climatic phenomenon, such as the Pineapple Express (PE), can significantly impact the disaster vicious cycle of flood, drought, and wildfires[10]. In the winter of 2005, the PE brought extreme precipitation from the Pacific tropics over the Hawaiian Islands to California causing widespread flooding. The abundant supply of water from these storms built up the biomass in the California chaparral, which became dry fuel in subsequent severe droughts, leading to the 2007 California wildfires. Fig. 2 presents the use of QSCAT SMC to monitor the impact of excessive PE activities in terms of the deposit and distribution of precipitation water on California land. In view of the recent extreme exacerbation of the water cycle, trends and statistics of SMC observed in this decade may better capture the recent climatic change while old statistics may not be applicable.

The utility of QSCAT to measure SMC becomes more critical in many regions of the world where surface measurements, either from rain gauges or surface radars, are limited or even non-existent for assessing the impact of severe storms or hurricanes on land, such as the identification and mapping of potential flood areas where soil saturation occurs. For a large cyclone or hurricane, the outer rain bands may reach land and deposit a large amount of precipitation water before the landfall occurs. This year (2008), Cyclone Nargis (01B, May 2008) was the worst disaster in Myanmar, causing catastrophic destruction and killing more than 140,000 people. Nargis developed in late April in the Bay of Bengal and made landfall on 2 May 2008 in Myanmar. Fig. 3 shows QSCAT SMC patterns on 29 April and 3 May 2008. As revealed by QSCAT, strong soil moisture increases already occurred extensively from Myanmar across Thailand and Cambodia on 29 May before Nargis made landfall. On 3 May, SMC was observed in areas further east to Laos and the border of Cambodia and Vietnam after landfall. It should be noted that Southeast Asia has large areas of tropical vegetation, and QSCAT is still capable to detect SMC from precipitation in several Southeast Asian countries.

4. THE CRYOSPHERE

The Earth's cryosphere spans over a vast expansion from extratropical regions to the poles. In this decade, drastic change has occurred in the cryosphere in the snow cover, ice sheets, and sea ice. Observations of the cryospheric environmental change using QSCAT have provided critical information on snowmelt patterns and Arctic sea ice reduction.

While data for snow extent, albedo, and water equivalent are available from various instruments[11, 12, 13], snowpack ripening is currently unavailable as a product. In this regard, QSCAT data are highly suited to this task, and an algorithm has been developed to detect areas of snow that are actively melting[14]. Nghiem and Tsai[14] showed the potential of the NASA scatterometer (NSCAT) data for applications to remote sensing of snow at the global scale, demonstrating that Ku-band backscatter is sensitive to snow properties and that onset of snowmelt can be detected using NSCAT data. Moreover, QSCAT data have been used to detect and map snowmelt[15]. At Ku-band frequency, QSCAT backscatter is highly sensitive to snow wetness. In wet snow, liquid water has an imaginary part that is three orders of magnitude larger than that of pure ice. Thus, a small amount of wetness can significantly change the imaginary part of the snow effective permittivity, and consequently decrease the backscatter.

To detect snowmelt, the diurnal difference method was first developed by Nghiem et al.[15]. A diurnal difference is defined as a relative quantity between morning and afternoon measurements in half a day. We co-locate the data from the early morning (t_a) in an ascending orbit pass and late afternoon (t_p) in a descending pass for each day. The diurnal backscatter change is defined as the backscatter difference in the decibel (dB) domain as $\Delta\sigma_{VV} = \sigma_{VV}(t_p) - \sigma_{VV}(t_a)$, where σ_{VV} is the vertical-polarization backscatter and all quantities are in dB. This algorithm has several advantages: independence of the scatterometer long-term gain drift, independence of the cross-calibration between QSCAT and future satellite scatterometers, independence of absolute backscatter from different snow classes and snow conditions,
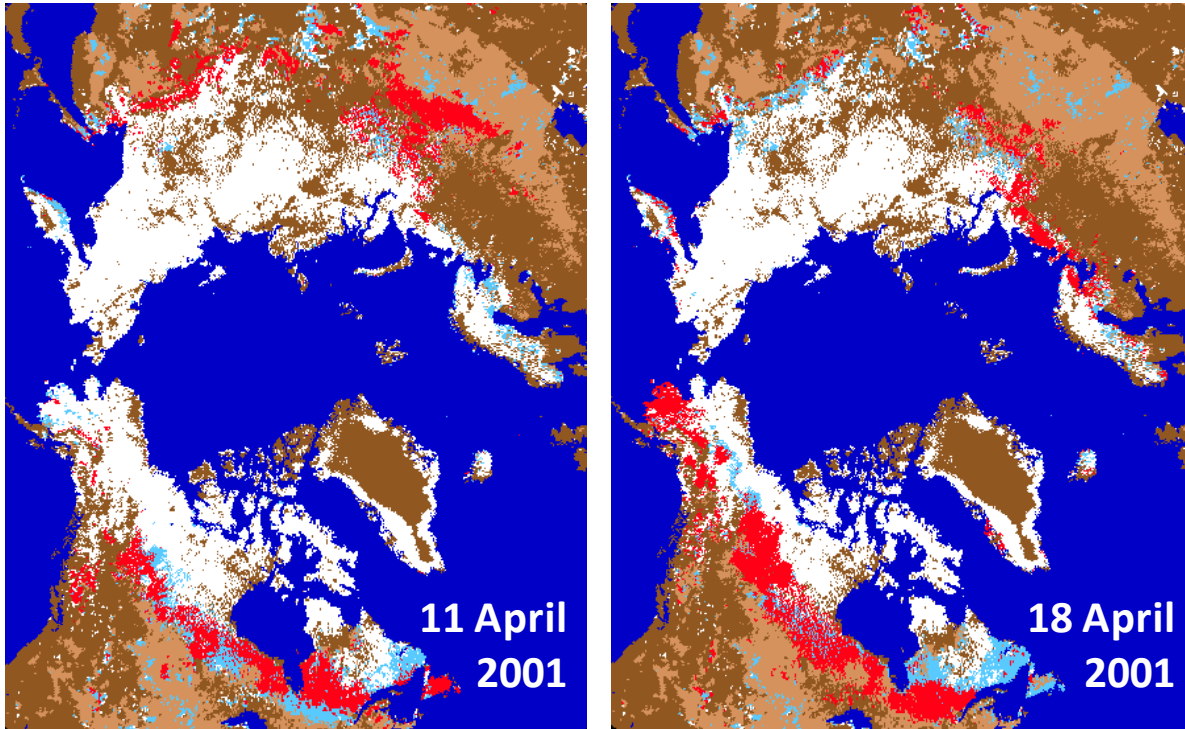
Fig. 4. QSCAT observations of snowmelt process of seasonal snow in the Northern Hemisphere on 11 April 2001 (left panel) and 18 April 2001 (right panel). The color code is: white for dry snow, red for active melt, light blue for reduced melt or refrozen snow, light brown for complete melt, brown for land, and blue for ocean.
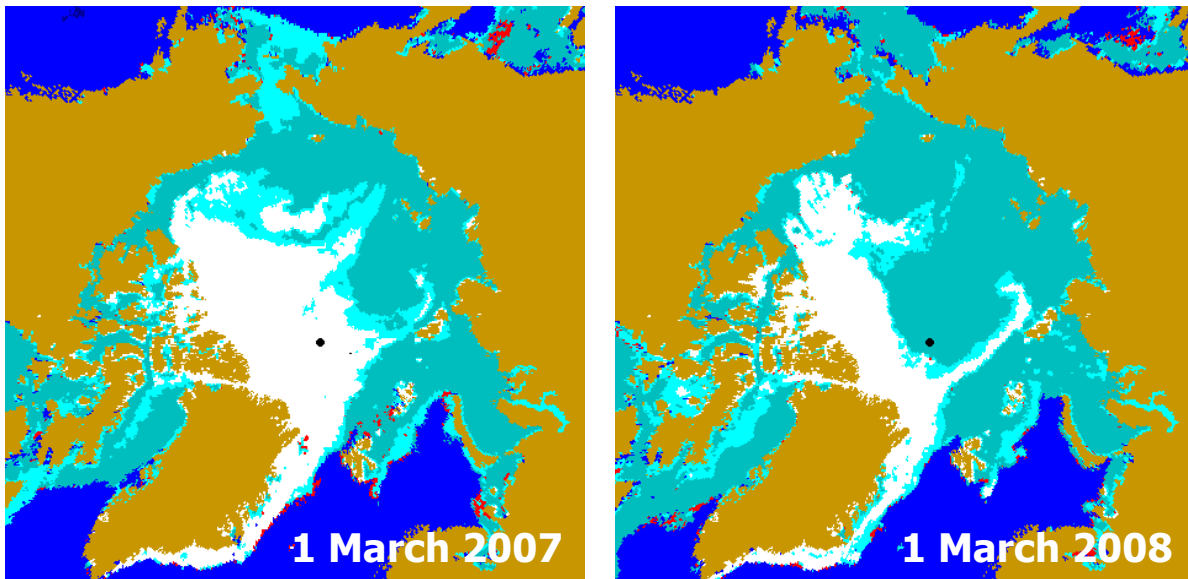

Fig. 5. Maps of Arctic sea ice derived from QSCAT data for 1 March 2007 (left panel) and 1 March 2008 (right panel). White is for perennial sea ice, aqua for mixed ice, turquoise for seasonal ice, red for melt on ice surface, blue for ice-free ocean, and brown for land. The black dot at the North Pole represents the size of a small disc of missing QSCAT data. This small missing-data disc allows daily accurate observations of the sea ice classes closest to the North Pole from satellite data.

and detection of both snow melt and refreezing. Fig. 4 includes a map of snowmelt process in the Northern Hemisphere on 11 April 2001 (left panel) and another snowmelt map one week later (right panel). The snowmelt maps in Fig. 4 show the northward migration of the melting process as expected: melt occurred at lower latitudes first and later at higher latitudes interlaced with periods of refreezing and melt recurrences. The snowmelt regime appeared as a coherent extensive longitudinal band as seen, for example, by the red band across the North American continent on 18 April 2001 (right panel in Fig. 4). The northern extent of this snowmelt band occurred approximately along the Canadian Shield from the west of Hudson Bay to the east of Yukon Territory. The evolution of the regional snowmelt process was not abrupt. In contrast, it exhibited periods of melting and refreezing as the snowmelt advanced northward. Animating daily time-series maps of snowmelt revealed cyclonic oscillations in snowmelt patterns over the continental scale.

QSCAT has enabled daily monitoring of Arctic perennial ice since its launch in 1999[16, 17]. QSCAT's unique features make it a powerful tool for mapping sea ice and accurately identifying sea ice conditions. It can distinguish sea ice from open water, differentiate classes of ice, and compensate for effects of strong winds on ocean surfaces and effects of melt on ice. Arctic sea ice mainly consists of perennial (multi-year) ice and seasonal (first-year) ice[18]. Seasonal ice forms each winter and melts the following summer, while perennial ice remains year round in the Arctic Ocean for several years to more than a decade. Seasonal sea ice is significantly thinner than perennial ice. As such, the perennial ice change is crucial to the overall stability of Arctic sea ice and has profound impacts on the Arctic environment. QSCAT results together with buoy observations showed that the extent of Arctic perennial sea ice (in March) was rapidly reduced at a rate of 1.5×10^6 km^2 per decade, triple the reduction rate during the three previous decades (1970-2000)[19]. Occupying the vast space vacated by perennial ice, the thinner and weaker seasonal ice has become the dominant ice class in the Arctic Ocean. This shift from the stable perennial ice to the weak seasonal ice has destabilized the Arctic environment.

A new record was set in the reduction of Arctic perennial sea-ice extent this winter, while the total sea ice extent has been stable compared to the average over the past nine years from QSCAT data. As of 1 March 2008, the extent of perennial sea ice was reduced by one million km^2 compared to that at the same time last year (Fig. 5). This reduction of perennial sea ice between the two years was about the size of Egypt, or Texas and California combined. This decrease of perennial ice continued the precipitous declining trend observed in this decade[18, 19]. The combination of the satellite and surface data records confirmed that the reduction of winter perennial-ice extent broke the record in 2008 compared to data over the last half century. Rather than melting, the loss of perennial ice extent in winter was driven by winds that compressed the ice and transported it out of Fram Strait (east of Greenland) and Nares Strait (west of Greenland). Another historical fact was that the boundary of perennial sea ice already crossed the North Pole in February 2008, leaving the area around the North Pole occupied by seasonal sea ice. This is the first time in the history of sea ice observations since the 1970s that observations indicate the seasonal ice migration into the NP area so early in winter. Furthermore, the sea-ice map on 1 March 2008 before the spring transition (right panel of Fig. 1) already revealed that seasonal ice resided in most of the Northern Sea Route, a vast region from Kara Sea and Laptev Sea to the North Pole, and most of the two routes of the Northwest Passage, north and south of Victoria Island, which facilitated the clearing of the waterways in summer 2008[20].

5. THE WORLD IN FOCUS

For almost a decade, QSCAT has provided a dataset with a high temporal resolution with near-daily coverage at low latitudes and coverage of two times per day at high latitudes, which is crucial to observe environmental change processes from diurnal responses to seasonal and interannual variability. While the high temporal resolution of QSCAT is required for many scientific studies and practical applications, a high spatial resolution, much better than 25 km (QSCAT cell data) or 12 km (QSCAT slice data), is desirable to observe urban and suburban environments and local-scale features such as persistent wind patterns on ocean surfaces around islands or in coastal regions. The inherent low resolution of QSCAT blurs small features, and an innovative method is necessary to obtain images with a focus for high spatial resolutions.

Traditionally, the deconvolution approach has been used to enhance the spatial resolution of backscatter data[21, 22, 23]. In the deconvolution approach, Álvarez-Pérez et al.[23] assume azimuthally independent radar echo, which is applicable to an isotropic area such as a forested area with vegetation randomly oriented in azimuth, but such an assumption is not valid for an azimuthally asymmetric urban area. The deconvolution approach requires that backscatter of the targeted area

remain unchanged during the time period of data acquisition for the resolution enhancement[24]. Such a requirement invalidates the resolution enhancement result for most environments undergoing natural processes (e.g., wind, snowmelt, precipitation, soil moisture change, flood, diurnal effects, etc.) that cause a backscatter change in the targeted area. For man-made targets (e.g., urban and suburban areas, etc.), backscatter change occurs even within a single orbit due to different azimuth angles with respect to the directional alignment of buildings, road networks, and infrastructures.

We have developed a new method[25] to achieve a high spatial resolution from QSCAT data, called the Dense Sampling Method (DSM). In the DSM formulation, the radar equation is cast in a form similar to the Radon transformation used in the medical Computed Tomography scan (CT scan). Unlike the CT scan method for stationary targets with unchanged characteristics, the challenge here is that both natural and man-made environments have changes causing backscatter to vary at all time scales (wind, rain, snow, flood, drought, new buildings, new parks, azimuth effects, etc.). To account for changes, the target signature is decomposed into a mean part and a fluctuation part. Then, a new transform called the rosette transform[25] is invented to utilize the multi-azimuth and multi-temporal data to obtain high-resolution results.

A simulation was completed to demonstrate the capability of DSM to identify and map city extent, urban and suburban boundary, commercial core within a city, and urban corridor[25]. Using the Príncipe Island (the famous test site where Eddington experimentally proved Einstein's theory of relativity using a solar eclipse in 1919[26]), the accuracy of DSM results is verified by an excellent agreement with geographical data of the location, shape, boundary, and extent of the island. The trade-off for the high spatial resolution obtained by DSM is the significant reduction in temporal resolution (e.g., annual or multi-annual periods). Thus, instead of observing transient processes, DSM is applicable to delineate urban extent and typology (e.g., commercial core versus residential areas) or to detect climatology conditions in natural environments.

DSM enables a new capability of QSCAT and future advanced high-resolution synthetic aperture scatterometers to address societal and environmental issues of our increasingly urban world: the global mapping and monitoring of land use in urban and suburban environments. The Night-Lights dataset obtained by the Defense Meteorological Satellite Program (DMSP) has been used as a proxy indicator of urban areas, which tend to overestimate urban-suburban areas, in what is known as an overglow[27]. However, there is no existing globally consistent data that delineate and characterize global land use and its change in urban and suburban environments at annual or multi-annual periods. Even in the data-rich U.S., census results are obtained at irregularly defined administrative units, once per decade, and are not intended to capture spatial dimensions of urban change processes. Yet, the state of the world's urban environments, consistently inventoried at fixed periods in time, is fundamental in addressing and solving many pressing policy questions grounded in the social and environmental sciences. This becomes more imperative not only as the world becomes more urban than rural, but also as more urban dwellers live in coastal zones, at risk of recent extreme catastrophic events such as the Asian Tsunami and Hurricanes Katrina and Rita[25].

We applied DSM, at a posting scale of 1 km, to a number of selected cities in different countries: United States, China, Bangladesh, Colombia, and Ecuador. DSM can detect and map city extent and city commercial and industrial core as illustrated in Fig. 6 for Phoenix (Arizona, U.S.) as an example. In Fig. 6, the high backscatter (red and white) physically corresponds to buildings and infrastructures in the city. The road network overlaid on the DSM map verifies the Phoenix urban extent (red-orange area), and the three-dimensional building overlay verifies the city commercial core (grey area). Moreover, our results showed that DSM backscatter is correlated with population density. The capability of backscatter to convey census information enables the use of radar data in socioeconomic research. Beyond urban and suburban environments, DSM is applicable to observations of natural environments containing persistent features, from cold regions to the tropics. The dual capability of DSM to observe both urban and natural regions is important for providing information consistently in time and in space, with a global data collection from the same sensor, to study urban changes and anthropogenic impacts on natural environments beyond the intermediate city surroundings. This was demonstrated by the use of DSM to identify a network of hydrological channels on the Greenland ice sheet and different vegetation biomes in central Africa[25]. Here, we show another use of DSM in the detection of wind shadows near islands, which is important to physical and biological oceanography and also for identifying aviation hazards (due to wind shear effects around wind shadow). Moreover, DSM can detect persistent patterns of higher wind speeds in offshore waters providing crucial information for the future development of offshore wind farms. Fig. 7 presents the delineation of both wind shadow and persistent high-wind patterns, at a spatial scale of 1 km, near the Hawaiian Islands in the Pacific Ocean. Results in the South Pacific showed that New Caledonia has a small wind shadow while the wind shadows of Vanuatu and Fiji are significantly larger.
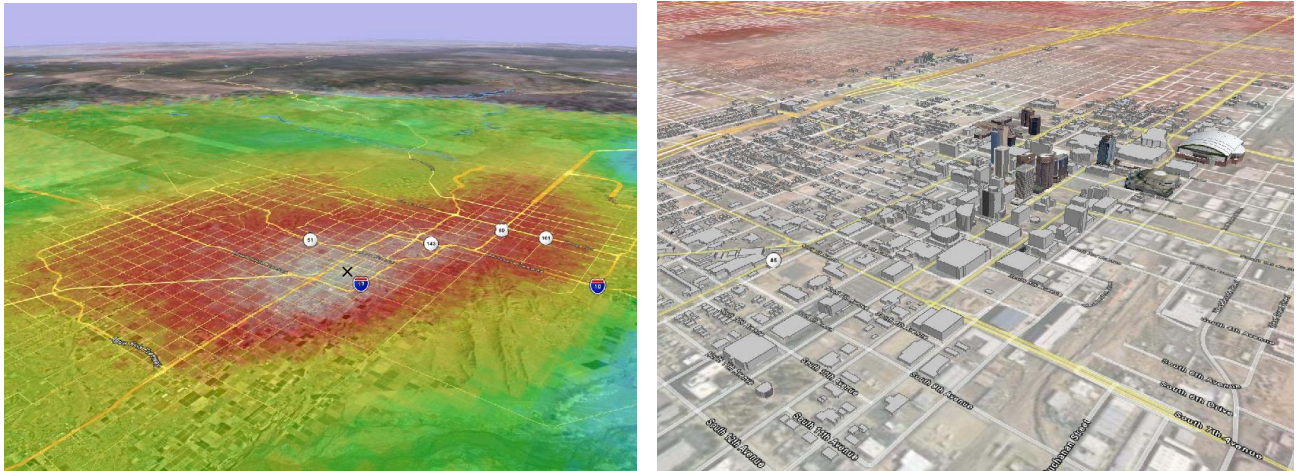
Fig. 6. DSM backscatter of Phoenix, Arizona (U.S.), with an overlay of road network (left panel) to verify the urban extent, and with an overlay of three-dimensional buildings (right panel) to verify the commercial and industrial core of the city. The symbol "X" on the left image is approximately the center of the commercial core shown in the right image.
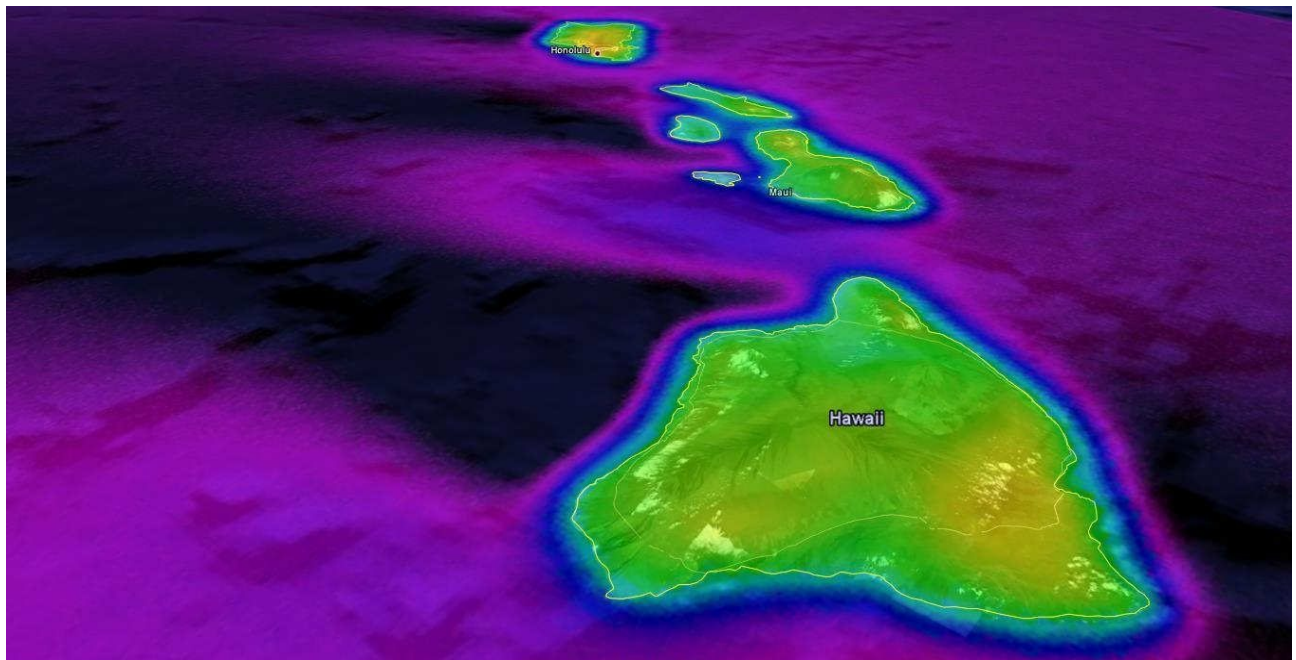

Fig. 7. Wind shadow areas (dark blue) near the Hawaiian Islands in the Pacific Ocean. The shadows locate on the leeward side of the islands with respect to the prevailing direction of the trade winds. For the Hawaii Island, a calm area is also observed on the windward side. An area of persistently high wind speeds is detected in the offshore area located between Hawaii and Maui and extended toward the southwest of these islands.

6. SUMMARY AND CONCLUSION

We have presented an overview of satellite scatterometry for remote sensing of the global environment on ocean, land, and ice using data from QSCAT.   Results include cyclone, hurricane, soil moisture, flood, drought, vegetation, snow,

sea ice, urban and suburban areas, wind shadow, and persistent wind patterns in offshore waters with different spatial and temporal scales.   Many of these results have contributed to Earth science studies as well as operational applications. With almost a decade of data, QSCAT can provide crucial results in a multitude of environmental parameters for the Global Earth Observation System of Systems.   As demonstrated, the capability of satellite scatterometry has been extended well beyond the original single objective of ocean wind measurement at coarse resolutions.   Thus, the value of future satellite scatterometer missions has been greatly elevated with direct and immediate contributions to Earth science studies as well as practical societal benefits.

ACKNOWLEDGMENTS

REFERENCES

[1]   Tsai, W.-Y., Nghiem, S. V., Huddleston, J. N., Spencer, M. W., Stiles, B. W. and West, R. D., "Polarimetric scatterometry: A promising technique for improving ocean surface wind measurements," IEEE Trans. Geosci. Remote Sens., 38(4), 1903-1921 (2000).

[2]   Nghiem, S. V., Liu, W. T., Tsai, W.-Y. and Xie, X., "Flood mapping over the Asian continent during the 1999 summer monsoon season," Proc. Int. Geosci. and Remote Sens. Symp., 5, 2027-2028 (2000).

[3]   United Nations, Office for the Coordination of Humanitarian Affairs, India - Cyclone OCHA Situation Report No. 9 (1999).

[4]   Choudhury, B. J., "Synergism of multispectral satellite-observations for estimating regional land-surface evaporation," Remote Sens. Environ., 49(3), 264-274 (1994).

[5]   Nghiem, S. V., Njoku, E. G., van Zyl, J. J. and Kim, Y., "Soil moisture variability pattern over continental extent observed with active and passive satellite data," Tech. Rep., JPL D-26225, 14 pp., Jet Propulsion Lab., California Inst. Tech. (2003).

[6]   Nghiem, S. V., Njoku, E. G., Brakenridge, G. R., and Kim, Y., "Land surface water cycles observed with satellite sensors," J6.14, Proc.19th Conference on Hydrology and 16th Conference on Climate Variability and Change, 85th Amer. Met. Soc. Meet. (2005).

[7]   Nghiem, S. V., "Advanced scatterometry for geophysical remote sensing," JPL Doc. D-23048, Jet Propulsion Lab., California Inst. Tech., Pasadena, California, (2001).

[8]   Moran, M. S., Vidal, V., Troufleau, D., Qi, J., Clarke, T. R., Pinter, Jr., P. J., Mitchell, T. A., Inoue, Y. and Neale, C. M. U., "Combining multifrequency microwave and optical data for crop management," Remote Sens. Environ., 61, 96-109 (1997).

[9]   Moran, M. S., Vidal, A., Troufleau, D., Inoue, Y. and Mitchell, T. A., "Ku- and C-band SAR for discriminating agricultural crop and soil conditions," IEEE Trans. Geosci. Remote Sens., 36, 265-272 (1998).

[10] Nghiem, S. V., "A disaster vicious cycle: Flood, drought, and wildfire," Report to NASA Earth Science - Applied Science Programs (2008).

[11] Hall, D. K. and Riggs, G. A., "Accuracy assessment of the MODIS snow-cover products," Hydrological Processes 21, 1534-1547 (2007).

[12] Kelly, R. E. J., Chang, A. T. C., Tsang, L. and Foster, J. L., "A prototype AMSR-E global snow area and snow depth algorithm," IEEE Trans. Geosci. Remote Sens., EO-1 Special Issue, 41(2), 230-242 (2003).

[13] Foster, J., Sun., C., Walker, J., Kelly, R., Chang, A., Dong, J. and Powell, H., "Quantifying the uncertainty in passive microwave snow water equivalent observations," Remote Sens. Environ., 94, 187-203 (2005).

[14] Nghiem, S. V. and Tsai, W. Y., "Global snow cover monitoring with spaceborne Ku-band scatterometer," IEEE Trans. Geosci. Remote Sens., 39, 2118-2134 (2001).

[15] Nghiem, S. V., Steffen, K., Kwok, R. and Tsai, W.-Y., "Detection of snow melt regions on the Greenland ice sheet using diurnal backscatter change," J. Glac., 47, 539-547 (2001).

[16] Nghiem, S. V., Van Woert, M. L. and Neumann, G., "Rapid formation of a sea ice barrier east of Svalbard," J. Geophys. Res., 110, doi:10.1029/2004JC002654 (2005).

[17] Nghiem, S. V. and Neumann, G., "Arctic sea-ice monitoring," 2007 McGraw-Hill Yearbook of Science and Technology, 12-15, McGraw-Hill, New York (2007).

[18] Nghiem, S. V., Chao, Y., Neumann, G., Li, P., Perovich, D. K., Street, T. and Clemente-Colón, P., "Depletion of perennial sea ice in the East Arctic Ocean," Geophys. Res. Lett., 33, L17501, doi:10.1029/2006GL027198 (2006).

[19] Nghiem, S. V., Rigor, I. G., Perovich, D. K., Clemente-Colon, P., Weatherly, J. W. and Neumann, G., "Rapid reduction of Arctic perennial sea ice," Geophys. Res. Lett., 34, L19504, doi:10.1029/2007GL031138 (2007).

[20] Nghiem, S. V., Rigor, I. G., Clemente-Colón, P., Perovich, D. K. and Neumann, G., "New record reduction of Arctic perennial sea ice in winter 2008," JPL Doc. D-44233, Jet Propulsion Lab., California Inst. Tech. (2008).

[21] Wang, Q. and Gogineni, S., "A numerical procedure for recovering scattering coefficients from measurements with wide-beam antennas," IEEE Trans. Geosci. Remote Sens. 29, 778-783 (1991).

[22] Long, D. G., Hardin, P .J. and Whiting, P. T., "Resolution enhancement of spaceborne scatterometer data," IEEE Trans. Geosci. Remote Sens., 33, 700-715 (1993).

[23] Álvarez-Pérez, J. L., Marshall, S. J. and Gregson, K., "Resolution improvement of ERS scatterometer data over land by Wiener filtering," Remote Sens. of Environ., 71, 261-271 (2000).

[24] Early, D. S. and Long, D. G., "Image reconstruction and enhanced resolution imaging from irregular samples," IEEE Trans. Geosci. Remote Sens., 39, 291-302 (2001).

[25] Nghiem, S. V., Balk, D., Ernesto, R., Neumann, G., Sorichetta, A., Small, C., and Elvidge, D. D., "Observations of urban and suburban environments with global satellite scatterometer data," to be published in Int. Soc. Photogram. and Remote Sens. (ISPRS) J. Photogram. and Remote Sens. (2008).

[26] Dyson, F. W., Eddington, A. S. and Davidson, C. R., "A determination of the deflection of light by the Sun's gravitational field from observations made at the total eclipse of May 29, 1919," Philosophical Transactions of the Royal Society of London, series A, 220, 291-330 (1920).

[27] Elvidge, C. D., Baugh, K. E., Kihn, E. A., Kroehl, H. W. and Davis, E. R., "Mapping city lights with nighttime data from the DMSP operational linescan system," Photo. Engineering Remote Sens.. 63, 727-734 (1997).